Journal of ELECTRONIC MATERIALS, Vol. 49, No. 6, 2020
https://doi.org/10.1007/s11664-020-08067-0
© 2020 The Minerals, Metals & Materials Society

Material Study of Co_2CrAl Heusler Alloy Magnetic Thin Film and Co_2CrAl/n-Si Schottky Junction Device

RASHMI SINGH,[1,4] FAIZAN AHMAD,[1] KASHIF NAZEER,[1] RACHANA KUMAR,[2] NARESH KUMAR,[3] ANIMESH K. OJHA,[3] SUNIL SINGH KUSHVAHA,[2] and PRAMOD KUMAR[1,5]

1.—Indian Institute of Information Technology Allahabad, Allahabad 211012, India. 2.—CSIR-National Physical Laboratory, New Delhi 110012, India. 3.—Department of Physics, Motilal Nehru National Institute of Technology Allahabad, Allahabad 211004, India. 4.—e-mail: rashmisingh8485@gmail.com. 5.—e-mail: pkumar@iiita.ac.in

The structural, optical, magnetic, and electrical properties of Co_2CrAl Heusler alloy magnetic thin films grown on n-type silicon (100) substrate (n-Si) and glass substrate were studied. The films were deposited using DC magnetron sputtering. X-ray diffraction (XRD) analysis confirmed the polycrystalline nature of the films. The effect of grain size on transmittance was investigated. Magnetic measurements revealed the presence of magnetic ordering in the films. Partial densities of states (PDOS) of the Co_2CrAl were calculated by density functional theory (DFT) methods using the Vienna Ab initio Simulation Package (VASP). Co_2CrAl thin film deposited over a silicon substrate was investigated for *I*–*V* characteristics. The electrical behaviour confirmed the existence of a Co_2CrAl/n-Si Schottky contact, which suggests a spin injection phenomenon from Co_2CrAl to n-Si by tunnelling through the lowered Schottky barrier.

Key words: Co_2CrAl Heusler alloy, magnetic thin films, spintronics, spin injection device, tunnelling, Schottky junction

INTRODUCTION

Over the past few decades, interest has increased in the use of complementary metal oxide semiconductors (CMOS) for fabrication of spin-based electronic (spintronic) devices.[1,2] Spin in semiconductors is crucial in terms of information processing in CMOS-based electronics. It has been suggested that spin-based devices offer a competitive advantage over conventional charge-based transistors in terms of power consumption and speed.[3] Such devices are required to be 100% spin-polarized; otherwise they result in inferior performance.[3,4] Theoretically, it has been established that improved spin injection efficiency at room temperature will contribute to many novel applications related to non-volatile memory storage and advanced computation.[4]

A number of studies have reported efficient spin injection from ferromagnetic metals such as Fe into semiconductors such as GaAs.[3] However, they have limitations related to low spin injection efficiency due to (1) impedance mismatch between the semiconductor and the ferromagnetic material, and (2) the limited spin polarization factor.[5–8] Experimental studies have also concluded that low spin injection efficiency is the result of certain detrimental features, i.e., (1) atomic disorder in the ferromagnetic layer, and (2) diffusion of magnetic impurities in the semiconductor.[3] Our aim in this study is to overcome these limitations for the fabrication of good spin injection devices.

In order to attain high (∼ 100%) spin polarization, the prospect of Heusler alloys as a spin injector layer has been explored.[9–13] Heusler alloys are ternary alloys that consist of interpenetrating face-centred cubic (fcc) lattices with the chemical

(Received September 13, 2019; accepted March 6, 2020; published online March 18, 2020)

formula X_2YZ for full-Heusler alloys and XYZ for half-Heusler alloys. Here, X and Y are the transition metals, and Z is usually either a semiconducting material such as Ge or Si, or a non-magnetic metal like Al. In the case of a fully ordered lattice $L2_1$, they consist of four interpenetrating fcc lattices, two of which are occupied by X atoms, while the other two are occupied by Y and Z atoms. If Y and Z sublattices are randomly intermixed, this gives rise to a disordered B2 phase. It has also been observed that certain Heusler alloys possess half-metallicity, i.e., all the carriers at the Fermi level are spin-polarized, and only the spin band is occupied.[9–13]

The formation of an $L2_1$ phase and suppression of a B2 phase is crucial to achieving half-metallicity in certain Heusler alloys, as they are ferromagnetic in nature and possess high Curie temperature ranging up to 1100°C.[14–16] High spin polarization has been observed in a Heusler alloy Co_2MnSi.[17] The $L2_1$ phase of Co_2CrAl is predicted to have high spin polarization and half-metallicity. These are crucial in order to maintain high spin injection despite interfacial strain effects.[18–20] Hence, it could potentially be utilized in their application as spin injectors and further employed in spintronic devices. In our present work, we deposited Co_2CrAl films on n-type silicon (100) substrate (n-Si)[21,22] and glass substrate[23] in order to study the properties of the film. We also tried to observe spin injection in the semiconductor (n-Si) by studying the Co_2CrAl/n-Si junction device. The thin films grown were characterized by different techniques so as to understand their structural, magnetic, optical, and electrical properties. To support the experimental results, the partial density of states (PDOS) of Co_2CrAl was calculated for the spin-up and spin-down electrons using the density functional theory (DFT) method with the help of Vienna Ab initio Simulation Package (VASP) code.[24–27]

METHODS

Thin films of Co_2CrAl were deposited on glass and n-type silicon (100) substrates (n-Si) of dimensions $\sim 2 \times 2$ cm, resistivity $\sim 5\ \Omega$ cm, and thickness $\sim 275\ \mu$m by DC sputtering for different deposition times. Before deposition, the substrates were cleaned by ultrasonication in deionized (DI) water for 10 min, followed by sonication in ethanol for another 10 min. Next, the substrates were dried under an argon (Ar) gas flow and then placed in the vacuum chamber of a sputtering system. The vacuum in the chamber was maintained at 4.0×10^{-3} Pa, and deposition was carried out for 25 min and 45 min, resulting in thickness of 100 nm and 140 nm, respectively. Sample codes 1 and 2 were given to the films deposited on glass substrates with thickness of 100 nm and 140 nm, respectively. Sample codes 3 and 4 were given to films deposited on silicon substrates with thickness of 100 nm and 140 nm, respectively. The deposition was followed by various characterization techniques. Cu–Kα_1 based x-ray diffraction (XRD) was performed in the range of $2\theta = 20° - 80°$ with a step size of 0.02°. Transmittance (T) % and reflectance (R) % in terms of the ratio of s- and p-polarized wave coefficients were measured to determine the optical parameters as well as the thickness of the film by ellipsometry (V-VASE ellipsometer and VB-400 ellipsometer control module, J.A. Woollam Company). A vibrating-sample magnetometer (VSM) (VersaLab cryogen-free VL096, Quantum Design) was used to study the magnetization properties of the Co_2CrAl thin films deposited on n-Si substrates.[28] Atomic force microscopy (AFM) (Agilent 5500, Agilent Technologies) was carried out in order to study the surface topology and morphology of the thin films. The band gap was calculated using Tauc plots.[29] Electrical current–voltage (I–V) measurements were performed using a Keithley 4200 semiconductor characterization system.

RESULTS AND DISCUSSION

The x-ray diffraction (XRD) analysis of samples 1, 2, 3, and 4 (Fig. 1) confirms the polycrystalline nature of the thin films. For all the films, the (220) phase seemed to be more dominant than the (400) phase, which is in good agreement with the results reported previously.[16] The dominant phase indicates the enhanced existence of the $L2_1$ ordered structure and suppressed B2 structure in the film.[20,30] These results confirmed the deposition of Co_2CrAl thin films on both the glass and n-Si substrates by sputtering.

AFM micrographs of samples 1 and 2 are shown in Fig. 2. It is observed that over an area of 4 μm^2, the roughness decreases with increasing thickness. This may be attributed to the increased grain size due to the rise in temperature inside the sputtering chamber during the growth of plasma.

The transmittance (T) % and reflectance (R) % ratios of the thin films in terms of s- and p-polarized wave coefficients were measured by ellipsometry, to determine the optical parameters as well as the thickness of the film. Optical transmittance is highly dependent on the grain size of the film.[19] When the grains are subjected to the oscillating electric field, it causes a tunnelling of charge carriers back and forth between the neighbouring grains.[19] These oscillations of the charge carriers are spin-dependent and contribute to magneto-optical and magneto-dielectric responses in the thin films.[17] This phenomenon is referred to as a tunnelling magneto-dielectric (TMD) effect.[17] Small oscillations were observed from the reflectance (R) % results of samples 3 and 4 for the film on n-Si.

Figure 3a shows the reflectivity R (%) graph in terms of the ratio of the reflection of polarized waves, i.e., R_p (p-polarized coefficient) and R_s (s-polarized coefficient), from Co_2CrAl thin films deposited on n-Si (samples 3 and 4) measured via

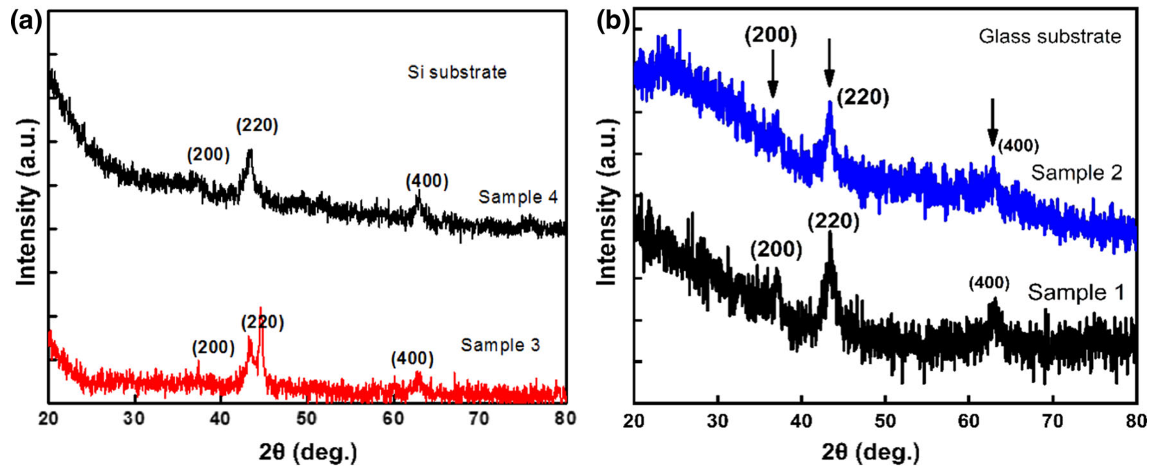

Fig. 1. (a) XRD of Co_2CrAl thin films deposited onto n-Si substrate of sample 3 and sample 4, (b) XRD of Co_2CrAl thin films deposited on glass substrate of sample 1 and sample 2.

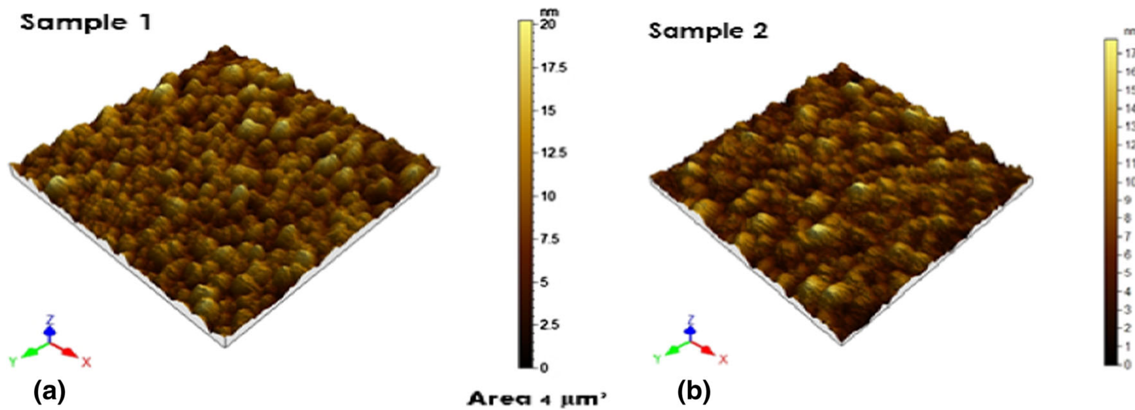

Fig. 2. AFM images of Co_2CrAl deposited on glass for (a) sample 1, (b) sample 2.

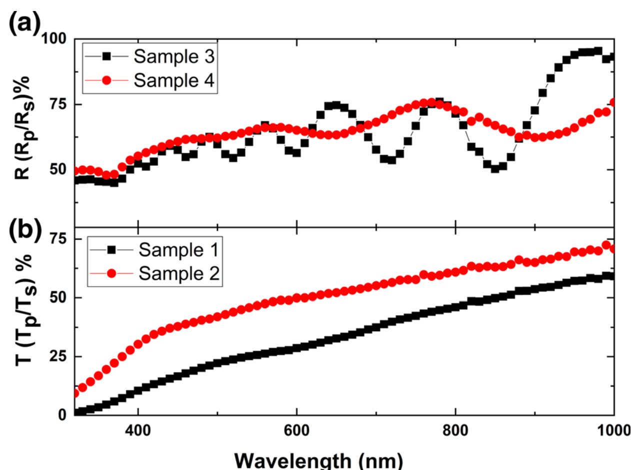

Fig. 3. (a) Reflectance (R) % ratio of Co_2CrAl thin films deposited on n-Si (samples 3 and 4). (b) Transmittance (T) % ratio for Co_2CrAl thin films deposited on glass substrate (samples 1 and 2).

ellipsometry in reflection mode. Figure 3b shows the transmittance T (%) graph in terms of the ratio of transmission of polarized waves, i.e., T_p (p-polarized coefficient) and T_s (s-polarized coefficient), from Co_2CrAl thin films deposited on glass substrates (samples 1 and 2) measured via ellipsometry in transmission mode. The range of wavelengths for the measurements was kept in the range of 300–1000 nm. The reflectance R (%) ratio of the thin film grown on n-Si was observed to be around 75–95% (Fig. 3a). The transmittance T (%) ratio was observed to be around 75–95% for the Co_2CrAl thin films grown on glass substrates (Fig. 3b).

The magnetization–hysteresis (M–H) curves of samples 3 and 4 at room temperature (300 K) are shown in Fig. 4. The magnetization of the films increases linearly with increasing magnetic field up to 2000 Oe, after which saturation occurs. These results are similar to those reported previously, where it was observed that as thickness increased, magnetization also increased due to increased coercivity.[31–33] There is a strong, nearly linear correlation between coercivity and grain size.[30–32] Upon increasing the film thickness, the grain size also increases, which enhances the chemical order as seen in the earlier studies.[31–33] Moreover, no new phase was evident from the XRD of the films (Fig. 1).

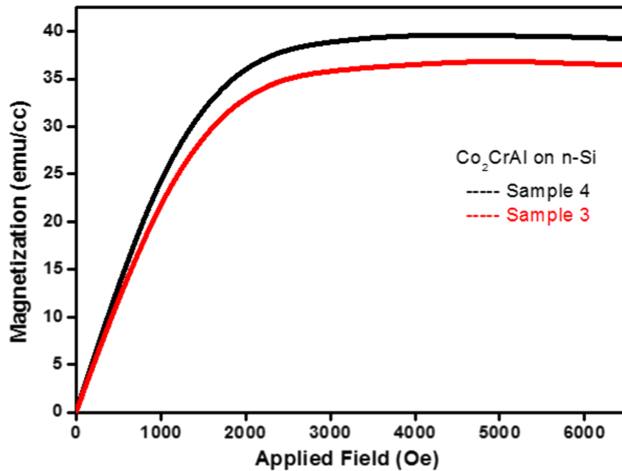

Fig. 4. Magnetization data for Co_2CrAl thin film for samples 3 and 4 on Si substrates.

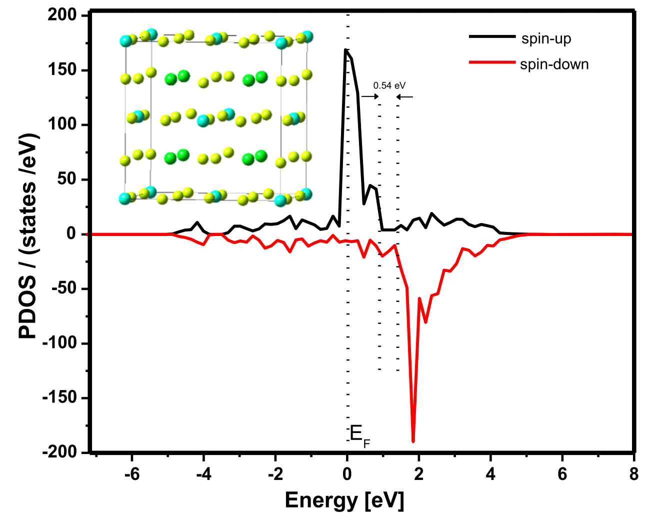

Fig. 5. The PDOS vs energy plot of Co_2CrAl calculated using VASP code. The optimized structure of Co_2CrAl is shown in the inset.

According to the studies on the band gap, the common 'd' band was completely filled in one spin sub-band. The 'd' peaks were present both above and below the Fermi level, where the minimum or zero density of states was found. The Fermi level was shifted to a different position, causing a difference in magnetic moment ($\mu \sim 4.8$–$6.0\ \mu$B).[14,15]

In order to understand the small band gap (0.51 eV) in Co_2CrAl thin films, the partial density of states (PDOS) of the electrons having up- and down-spins in the crystal lattice was calculated by the density functional theory (DFT) method using VASP code.[27–34] The calculation was performed using generalized gradient approximation–Perdew–Burke–Ernzerhof exchange energy (GGA–PBE) exchange–correlation functional. This is a spin-polarized magnetic calculation using 'normal' precision and a default plane wave cut-off energy of 267.968 eV. The electronic iteration convergence was 0.0004 eV using the very fast residual minimization scheme–direct inversion in the iterative subspace (RMM-DIIS) algorithm and reciprocal space projection operators. Explicit k-mesh of 4x4x4 was used. This corresponds to actual k-spacing of $0.156 \times 0.156 \times 0.156$ per angstrom. The k-mesh was forced to be centred on the gamma point. We selected the proper LORBIT tag in the INCAR file (e.g. LORBIT = 11 tag) to obtain the spd decomposed DOSCAR file output. In Fig. 5, it is important to note that the density of electrons with up-spin peaks at 0.015 eV, i.e., almost at the Fermi energy, with density 167.80 states/eV. However, the density of electrons with spin-down peaks at 1.88 eV, which is slightly removed from the Fermi level and with energy density 189.47 states/eV. The observed magnetic nature of Co_2CrAl film may be explained in terms of the difference in the density of spin-up and spin-down electrons ($\sim$ 22 states/eV) as calculated theoretically.

DEVICE APPLICATION

Figure 6a shows a schematic of the fabricated devices. Multiple devices were fabricated with different electrodes, and *I–V* was measured with voltage ranging from -5 V to 5 V (Fig. 6b). The fabrication of the junction device was carried out by adopting the procedure of masking and contacts as reported in Faizan et al.[35]. In the forward bias region ($V > 0$), the current varies non-linearly with voltage. The spin injection from Co_2CrAl into n-Si can be described in the reverse bias region ($V < 0$) as the current is described by the field emission process at lower temperatures.[36,37]

The leakage current of the Co_2CrAl/n-Si junction in the reverse bias region ($V < 0$, spin-detection condition) showed a significant increase. Consequently, the *I–V* plots of contacts with Co_2CrAl are symmetric. Co_2CrAl is a half-metallic ferromagnet (HMF), which implies that it acts as a metal for an electron having a specific spin direction and as a semiconductor for an electron having another spin direction.[38,39] The *I–V* characteristics can be explained on the basis of Schottky barrier formation at the junction of Co_2CrAl/n-Si.[21]

Figure 7 shows the band diagram modelling of the Co_2CrAl thin film and n-Si junction. A Schottky barrier was formed at the junction of an n-Si semiconductor and Co_2CrAl, considering it as a metal[36] having a work function greater than the n-Si.[34] In Fig. 7a, initial band diagrams for the Co_2CrAl film and the n-Si semiconductor are shown separately before junction formation. Here, E_v and E_c are the valence band (VB) and the conduction band (CB) of the n-Si, respectively. E_{FS} and E_{FM} denote the Fermi levels of n-Si and Co_2CrAl, respectively. The $e\phi_s$ and $e\phi_m$ are the work function of n-Si and of the Co_2CrAl thin film, considering $e\phi_m > e\phi_s$.[34] Also, e_χ is the electron affinity for n-Si. When the Co_2CrAl film with work function $e\phi_m$

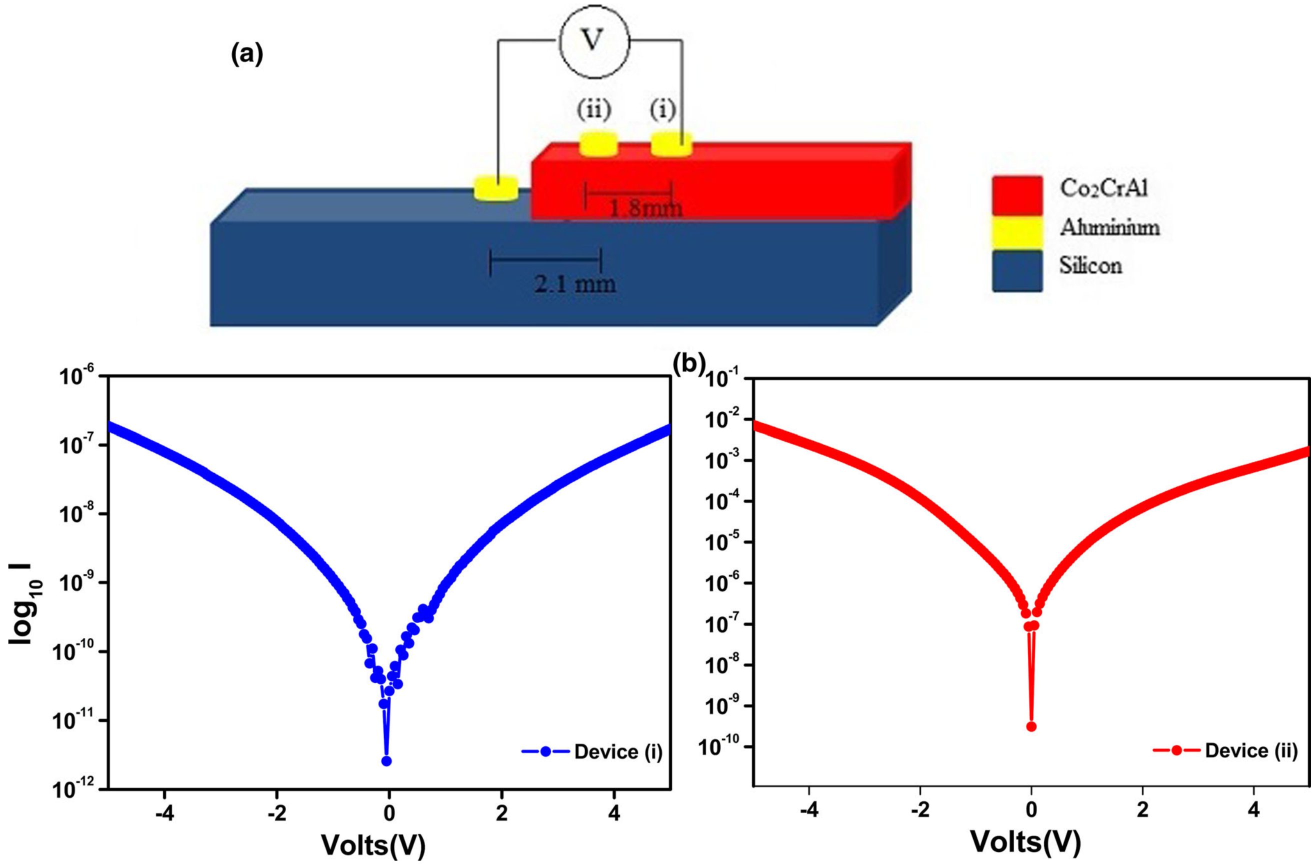

Fig. 6. (a) Schematic of Co_2CrAl/n-Si junction device structure, (b) *I–V* results of device (i) and device (ii) for applied voltage bias from −5 V to 5 V.

comes in contact with the n-Si semiconductor having a work function $e\phi_s$, charge transfer occurs and the Fermi levels are aligned until equilibrium is attained, as shown in Fig. 7b. The equilibrium contact potential V_0 prevents further electron diffusion from the conduction band into the Co_2CrAl film and is equal to the difference ($\phi_m - \phi_s$). The ϕ_{SB} is the potential barrier height for electron injection from Co_2CrAl film to n-Si. Figure 7c shows the junction when forward biased. When negative voltage is applied to n-Si with respect to the Co_2CrAl film, the electrostatic potential shifts to a lower value (V_0–V) from V_0 with respect to the Co_2CrAl, resulting in the lowering of the barrier for the injection of majority carriers (electrons) in forward biasing. The current in forward biasing is mainly due to majority carrier injection (electrons), while the minority carrier injection is very small or absent as compared with conventional Schottky diodes, and reduces the charge delays. The storage charge delay is an important feature of a Schottky barrier diode. The current in forward bias of our Schottky diode is equivalent to the diode current given by the equation:

$$I = I_0(e^{eV/kT} - 1) \quad (1)$$

Here, I_0 is the saturation current, k the Boltzmann constant, and V the forward voltage.

Figure 7d shows the reverse biasing of the junction. A reverse bias increases the barrier to $V_0 + V$, and the electron flow from n-Si to Co_2CrAl is negligible. The flow of electrons from the Co_2CrAl film to the n-Si semiconductor is obstructed by the barrier (ϕ_m–χ). However, the similar currents observed in the reverse biased condition can be attributed to the presence of up-spin near the n-Si semiconductor and Co_2CrAl (SC- HMF) junction.[40–42] The presence of up-spin at the n-Si/Co_2CrAl junction lowers the Schottky barrier ϕ_{SB} and allows the electrons to tunnel through the barrier, towards the semiconductor. The saturation current is dependent on the size of the barrier ϕ_{SB} for electron injection from the Co_2CrAl film to the n-Si, whereas ϕ_m–χ remains unaffected by the bias voltage applied. The reverse saturation current I_0 is given by:

$$I_0 \propto e^{-e_{SB}/kT} \quad (2)$$

The Schottky behaviour of the Co_2CrAl/n-Si heterojunction is a consequence of Co_2CrAl forming a Schottky junction with n-Si. Lowering of the Schottky barrier Φ_{SB} can be attributed to the doping

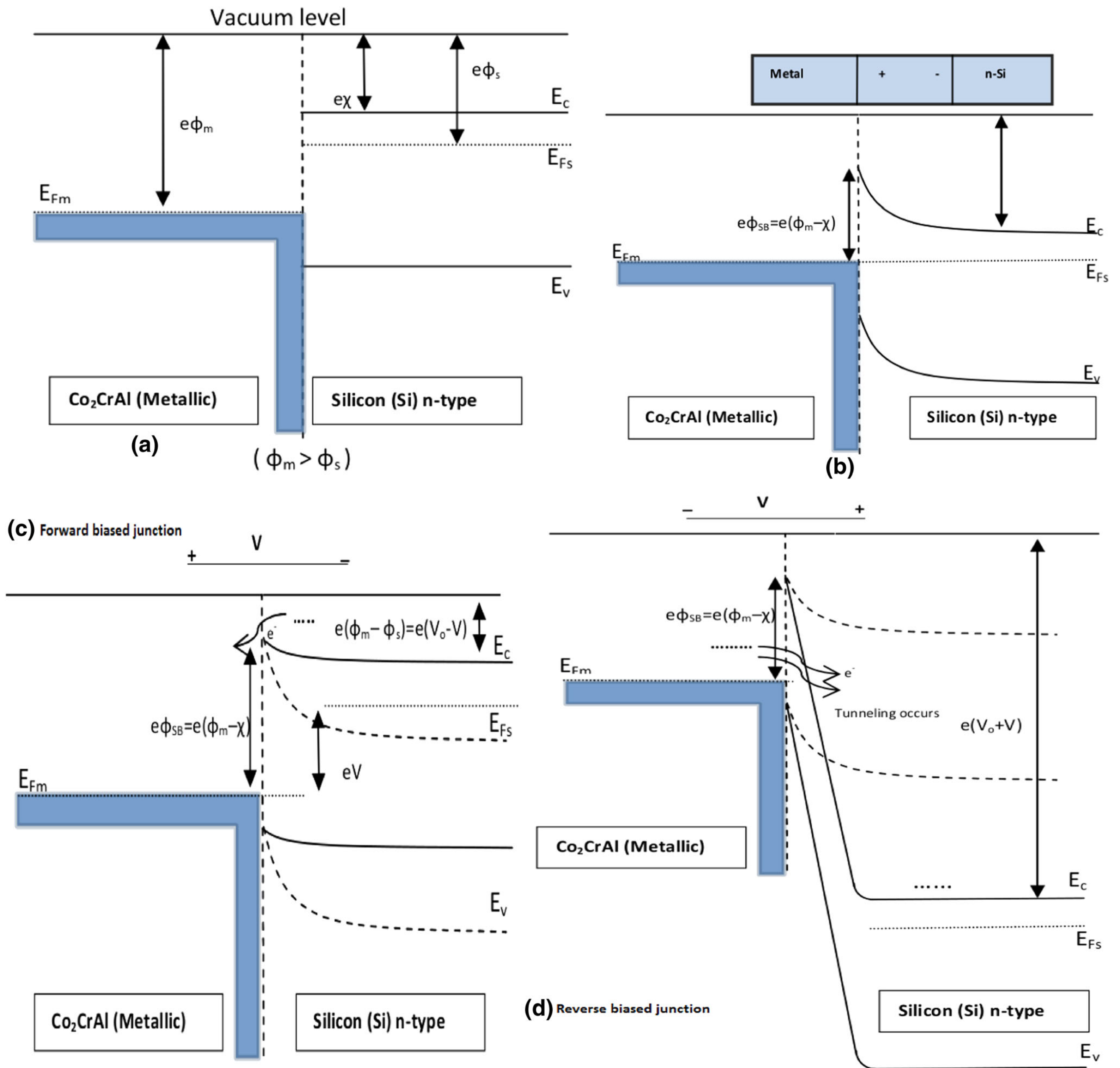

Fig. 7. Energy bands of junction Co_2CrAl/n-Si (a) initial and (b) final alignment of Fermi levels under equilibrium, (c) forward biased and (d) reverse biased.

of the semiconductor substrate or the smaller work function Φ_B of the metallic part in comparison with the substrate.[34,43] However, in our study, the substrate was not doped and the work function Φ_B of the film was not less than that of the substrate.[34,43] As Sughara et al. showed in an earlier work, the presence of up-spin near the semiconductor–HMF junction caused lowering of the Schottky barrier Φ_{SB}, allowing it to tunnel through the semiconductor, thus resulting in spin injection.[40–42] Hence, it can be inferred that due to the application of reverse bias voltage, electrons possessing the up-spin tunnel through the n-Si by lowering of the Schottky barrier. Figure 7d depicts the band diagrams for the Co_2CrAl and n-Si junction after application of reverse bias voltage. We observed that current varies inversely with the distance between electrodes, used for measuring the *I–V* for different devices. Its explanation can be found by the optimization of the devices in terms of the ideality factor and figure of merit, as observed for Schottky devices of varying geometry.[44] It was also concluded therein that the series and contact resistance were reduced for a device having reduced inter-electrode distances, which was due to the smaller dimensions under consideration.[44]

CONCLUSION

Co_2CrAl belongs to a family of full-Heusler alloys known to be half-metallic ferromagnets. This implies that it acts as a semiconductor for a specific spin and as a metal for another spin. We have investigated structural, optical, magnetic, and electrical properties of Co_2CrAl Heusler alloy magnetic thin films. We observed an indirect forbidden transition band gap for Co_2CrAl and its metallic behaviour simultaneously by observing its spin injection from Co_2CrAl to n-Si. The *I–V* results of the Co_2CrAl/n-Si junction device showed flow of increased leakage current in the reverse bias region, which can be attributed to the presence of up-spin electrons, resulting in the lowering of the semiconductor-HMF Schottky barrier, allowing it to tunnel through the semiconductor. This was responsible for the tunnelling of up-spin electrons from the HMF to the semiconductor. Our observations may aid in the development of better spin injection devices based on Co_2CrAl with improved material properties. Such devices may be utilized for high-speed applications.

ACKNOWLEDGMENT

We would like to thank DST, Govt. of India for financial support. We would like to acknowledge CIR, MNNIT Allahabad for the experimental and characterization support. Special thanks to Professor K.G. Suresh from IIT Bombay, Mumbai (India), for helping us in proofreading the final version of the manuscript.

REFERENCES

1. V.K. Joshi, *ScienceDirect* 19, 1503 (2011).
2. S.A. Wolf, D.D. Awschalom, R.A. Buhrman, J.M. Daughton, S.V. Molnár, M. Roukes, A.Y. Chtchelkanova, and D.M. Treger, *Science* 294, 1488 (2001).
3. S. Bandyopadhyay and M. Cahay, General principles of spin transistors and spin logic devices.*Handbook of spintronics*, ed. Y. Xu, D. Awschalom, and J. Nitta (Dordrecht: Springer, 2011), p. 1175.
4. Q.L. Ma, X.M. Zhang, T. Miyazaki, and S. Mizukami, *Sci. Rep.* 5, 7863 (2015).
5. L. Tang and Z. Yang, *J. Appl. Phys.* 114, 193703 (2013).
6. S. Husain, S. Akansel, A. Kumar, P. Svedlindh, and S. Chaudhary, *Sci. Rep.* 6, 28692 (2016).
7. C. Felser and G.H. Fecher, *Spintronics: from materials to devices* (Dordrecht: Springer, 2013).
8. I. Galanakis, Theory of Heusler and Full-Heusler Compounds.*Heusler Alloys*, Vol. 222, ed. C. Felser and A. HirohataSpringer Series in Materials Science, (Cham: Springer, 2016), .
9. F. Mott, *Proc. Roy. Soc.* A153, 699 (1936).
10. R.Y. Umetsu, K. Kobayashi, A. Fujita, K. Oikawa, R. Kainuma, K. Ishida, N. Endo, K. Fukamichi, and A. Sakuma, *Phys. Rev. B: Condens. Matter Mater. Phys.* 72, 214412 (2005).
11. S. Wurmehl, G.H. Fecher, K. Kroth, F. Kronast, H.A. Dürr, Y. Takeda, Y. Saitoch, K. Kobayashi, H.I. Lin, G. Schönhense, and C. Felser, *J. Phys. D Appl. Phys.* 39, 803 (2006).
12. J. Kubler, G.H. Fecher, and C. Felser, *Phys. Rev. Condens. B: Matter Mater. Phys.* 76, 024414 (2007).
13. H.C. Kandpal, G.H. Fecher, and C. Felser, *J. Phys. D Appl. Phys.* 40, 1507 (2007).
14. M. Hakimi, P. Kameli, and H. Salamati, *J. Magn. Magn. Mater.* 322, 3443 (2010).
15. R. Apetz and M.P.B. Van Bruggen, *J. Am. Ceram. Soc.* 86, 480 (2003).
16. T.C. Wen and D.K. Shetty, *Proc. of SPIE* 7302, 73020Z-1 (2009).
17. N. Kobayashi, H. Masumoto, S. Takahashi, and S. Maekawa, *Sci. Rep.* 6, 34227 (1–7) (2016).
18. J. Inoue and S. Maekawa, *Phys. Rev. B* 53, Article R11927 (R) (1996).
19. S. Mitani, H. Fujimori, and S. Ohnuma, *J. Magn. Magn. Mater.* 165, 141 (1997).
20. A. Hirohata, H. Kurebayashi, S. Okamura, M. Kikuchi, T. Masaki and T. Nozaki, *J. Appl. Phys.* 97, Article 103714 (2005).
21. A. Dankert, R.S. Dulal, and S.P. Dash, *Sci. Rep.* 3, 3196 (2013).
22. F. Rortais, C. Vergnaud, C. Ducruet, C. Beigne, A. Marty, J.P. Attane, J. Widiez, H. Jaffres, J.M. George, and M. Jamet, *Phys. Rev. B* 94, 174426 (2016).
23. W. Han, Y. Otani, and S. Maekawa, *NPJ Quantum Mater.* 3, 27 (2018).
24. G. Kresse and J. Furthmüller, *Phys. Rev. B* 54, 11169 (1996).
25. G. Kresse and J. Furthmüller, *Comput. Mater. Sci.* 6, 15 (1996).
26. A. Kumar, A. Singh, and A.K. Ojha, *J. Phys. Chem. C* 123, 13385 (2019).
27. D.P. Rai, A. Shankar, Sandeep, M.P. Ghimire, and R.K. Thapa, *Int. J. Mod. Phys. B* 26, 1250071 (2012).
28. J. Dubowik, I. Gościańska, K. Załęski, Y. Kudryavtsev, and Y. Lee, *Acta Phys. Pol. A* 115, 360 (2009).
29. A. Tumuluri, K.L. Naidu, and K.C.J. Raju, *Int. J. ChemTech Res.* 6, 3353 (2014).
30. X. Dai, M. Joudan, and C. Felser, *J. Phys. D: Appl. Phys.* 42, 084014 (2009).
31. M.F. Toney, W.Y. Lee, J.A. Hedstrom, and A. Kellock, *J. Appl. Phys.* 93, 9902 (2003).
32. C. Yang, B. Liu, G. Liu, F. Diao, H. Yang, and Y. Wang, *Solid State Ionics* 319, 28 (2018).
33. S. Singh, P.K. Tyagi, and H.K. Singh, *AIP Adv.* 8, 095002 (2018).
34. M. Jourdan, F. Große-Schulte, M. Hahn, and G. Schönhense, *J. Phys. D: Appl. Phys.* 44, 155001 (2011).
35. F. Ahmad, R. Singh, P.K. Misra, N. Kumar, R. Kumara, and P. Kumar, *J. Electron. Mater.* 47, 6972 (2018).
36. B. Min, K. Motohashi, C. Lodder, and R. Jansen, *Nat. Mater.* 5, 817 (2006).
37. G. Schmidt and L.W. Molenkamp, *Semicond. Sci. Technol.* 17, 310 (2002).
38. R. Farshchi and M. Ramsteiner, *J. Appl. Phys.* 113, 91101 (2013).
39. M. Zhang, Z. Liu, H. Hu, G. Liu, Y. Cui, J. Chen, G. Wu, X. Zhang, and G. Xiao, *J. Magn. Magn. Mater.* 277, 130 (2004).
40. S. Sugahara and M. Tanaka, *Appl. Phys. Lett.* 84, 2307 (2004).
41. N.L. Chung, M.B.A. Jalil, and S.G. Tan, *J. Appl. Phys.* 108, 034503 (2010).
42. S. Sugahara and M. Tanaka, *Physica E* 21, 996 (2004).
43. Y. Ando, K. Hamaya, K. Kasahara, Y. Kishi, K. Ueda, K. Sawano, T. Sadoh, and M. Miyao, *Appl. Phys. Lett.* 94, 182105 (2009).
44. I.A. Amatalo, N.E. Makori, J. Maera, D. Wamwangi, and P.M. Karimi, *Microelectron. Solid State Electron.* 3, 11 (2014).

Publisher's Note Springer Nature remains neutral with regard to jurisdictional claims in published maps and institutional affiliations.